applied optics

Analysis of nodal aberration properties in off-axis freeform system design

HAODONG SHI,[1,*] HUILIN JIANG,[1] XIN ZHANG,[2] CHAO WANG,[2] AND TAO LIU[2]

[1]Institute of Space Optoelectronics Technology, Changchun University of Science and Technology, Changchun 130022, China
[2]Key Laboratory of Optical System Advanced Manufacturing Technology, Changchun Institute of Optics, Mechanics and Physics, Chinese Academy of Sciences, Changchun 130033, China
*Corresponding author: shihaodong08@163.com

Received 25 May 2016; revised 29 July 2016; accepted 29 July 2016; posted 1 August 2016 (Doc. ID 266517); published 18 August 2016

Freeform surfaces have the advantage of balancing off-axis aberration. In this paper, based on the framework of nodal aberration theory (NAT) applied to the coaxial system, the third-order astigmatism and coma wave aberration expressions of an off-axis system with Zernike polynomial surfaces are derived. The relationship between the off-axis and surface shape acting on the nodal distributions is revealed. The nodal aberration properties of the off-axis freeform system are analyzed and validated by using full-field displays (FFDs). It has been demonstrated that adding Zernike terms, up to nine, to the off-axis system modifies the nodal locations, but the field dependence of the third-order aberration does not change. On this basis, an off-axis two-mirror freeform system with 500 mm effective focal length (EFL) and 300 mm entrance pupil diameter (EPD) working in long-wave infrared is designed. The field constant aberrations induced by surface tilting are corrected by selecting specific Zernike terms. The design results show that the nodes of third-order astigmatism and coma move back into the field of view (FOV). The modulation transfer function (MTF) curves are above 0.4 at 20 line pairs per millimeter (lp/mm) which meets the infrared reconnaissance requirement. This work provides essential insight and guidance for aberration correction in off-axis freeform system design.

OCIS codes: (080.1010) Aberrations (global); (080.4228) Nonspherical mirror surfaces; (220.1250) Aspherics.

http://dx.doi.org/10.1364/AO.55.006782

1. INTRODUCTION

Due to the limitations of traditional rotationally symmetric reflective systems, an off-axis optical system was designed to remove the obscuration for increasing the total intensity of light [1]. Several strategies can be employed to obtain an off-axis system, such as (1) the aperture stop can be offset from the mechanical axis, (2) the biased field of view (FOV) can be optimized, (3) the surfaces themselves can be tilted [2]. In most cases, the third method is seldom adopted because of the near-field constant astigmatism and coma aberrations induced by tilting surfaces. These kinds of aberrations may not be easily corrected by conventional rotationally symmetric surfaces. However, the freeform surfaces provide greater control to the off-axis aberrations than the rotationally symmetric surfaces. Additionally, with the development of computer-controlled machining processes, freeform surfaces are no longer prohibitive [3]. Based on the above reasons, freeform surfaces are widely used in off-axis system design.

Because the traditional aberration theory is not appropriate for the freeform system anymore, optical designers lack intuitive insights on the contribution of aberrations induced by the freeform surfaces. Until recently, Fuerschbach *et al.* derived expressions for the aberration theory of systems with freeform surfaces described by Zernike polynomials [4]. The theory built upon the vector aberration theory (VAT) introduced by Thompson [5]. Based on the work of Fuerschbach, Yang analyzed the nodal aberration properties of Zernike polynomial surfaces in a coaxial imaging system [6]. However, the total third-order wave aberration expressions when the freeform surfaces were introduced into an off-axis system were not derived. The relationship between the freeform shape and the off-axis acting on the aberration nodal position was not revealed either. In order to provide essential guidance for off-axis aberration correction when using freeform surfaces, the contribution of freeform surfaces in an off-axis system needs to be developed urgently.

This paper is organized as follows: in Section 2, the wave aberration formulations are derived for an off-axis system including freeform surfaces described by Zernike polynomials. When each Zernike term is added to an off-axis system, the nodal properties of astigmatism and coma are analyzed in detail. The relationship between the off-axis and surface shape acting on the nodal distributions is revealed for the first time. The full-field displays (FFDs) generated by CODE V are utilized to validate the derivation. In Section 3, in order to demonstrate the applicability of the theoretical derivations, an optical system with two tilted Zernike mirrors is optimized. The first-order starting point parameters are considered and computed according to basic mechanical requirements. In order to balance the field constant aberrations induced by tilting surfaces, the node-based analysis approach is employed in the optimization process of the optical design. The strategy of selecting Zernike terms is guided by the off-axis freeform aberration distribution discussed in Section 2. The design results and the imaging performance of the off-axis freeform system, which works in the long-wave infrared spectrum (8 ~ 12 μm), are reported at the end of this section. Conclusions are finally given in Section 4.

2. NODAL ABERRATION PROPERTIES OF FREEFORM SURFACES IN AN OFF-AXIS SYSTEM

In order to account for the effects of tilt and decenter perturbations on the wave aberration expansion for a rotationally symmetric optical system completely, Thompson presented a vector formulation of wave aberration [5]. By inducing the field decentration vector $\vec{\sigma}_j$, which determined the center of each surface contribution in the image plane, the wave aberration expansion to the third-order, including decenters and tilts, can be expressed as

$$\begin{aligned} W = {} & \Delta W_{20}(\vec{\rho}\cdot\vec{\rho}) + \Delta W_{11}(\vec{H}\cdot\vec{\rho}) + \sum_j W_{040_j}(\vec{\rho}\cdot\vec{\rho})^2 \\ & + \sum_j W_{131_j}[(\vec{H}-\vec{\sigma}_j)\cdot\vec{\rho}](\vec{\rho}\cdot\vec{\rho}) \\ & + \sum_j W_{222_j}[(\vec{H}-\vec{\sigma}_j)\cdot\vec{\rho}]^2 \\ & + \sum_j W_{220_j}[(\vec{H}-\vec{\sigma}_j)\cdot(\vec{H}-\vec{\sigma}_j)](\vec{\rho}\cdot\vec{\rho}) \\ & + \sum_j W_{311_j}[(\vec{H}-\vec{\sigma}_j)\cdot(\vec{H}-\vec{\sigma}_j)][(\vec{H}-\vec{\sigma}_j)\cdot\vec{\rho}], \end{aligned} \tag{1}$$

where $\vec{H}$ denotes a normalized vector for the field height in the image plane, and $\vec{\rho}$ denotes a normalized vector describing the position in the pupil. The subscript j is the index for the summation over each optical surface. Here, the wave-front focus (ΔW_{20}) and tilt (ΔW_{11}) are induced for completeness, which will not be considered in the following discussion. The rest of the terms, W_{040}, W_{131}, W_{222}, W_{220}, and W_{311}, denote the third-order of spherical aberration, coma, astigmatism, field curvature, and distortion according to their ranks, respectively. The coefficient of each term will not be affected by tilts and decentrations. Due to the introduction of vector $\vec{\sigma}_j$, the aberrations' field dependence behaviors have been perturbed. Consequently, the locations and the amount of zero aberration (nodal) will be changed.

In the numerous descriptions of optical freeform surfaces, Zernike polynomials have a close relationship with the wavefront expansion terms. They allow designers to directly leverage the optical design insight provided by VAT [5,7]. Additionally, Zernike polynomials are widely used in the existing commercial optical design software, such as CODE V [8]. Therefore, the aberration distribution of the freeform surfaces described by Zernike polynomials is mainly discussed. There are two parts in the Zernike polynomial expressed in Eq. (2). One is the basic shape for extracting the spherical/aspheric contribution, the other is the expansion polynomial with coefficients.

$$Z = \frac{c(x^2+y^2)}{1+\sqrt{1-(1+k)c^2(x^2+y^2)}} + \sum_{i=1}^{n} C_i Z_i(\rho,\theta), \tag{2}$$

where c is the surface curvature, k is the conic constant, Z_i is the ith Zernike polynomial, and C_i is the corresponding coefficient. The Fringe Zernike polynomial form is applied in this paper because it could correspond with the traditional Seidel aberration. It is important to recognize that the Zernike polynomial portion is the mainly perturbing source of the asymmetric aberration distribution. So, we mainly focus on discussing the aberration properties introduced by various Fringe Zernike polynomial terms.

It is critical to realize that the aberration contributed by freeform surfaces is not only indicated by surface shape, but also by the location of the stop [4]. Fuerschbach and Yang have investigated the aberration distribution when the Fringe Zernike terms were added to the nonstop surface in a coaxial system [4,6]. The modified pupil vector $\vec{\rho}'$ relates the beam displacement vector $\Delta\vec{h}$ to the original pupil vector $\vec{\rho}$. The vector $\Delta\vec{h}$ is proportional to $\vec{H}$ in a small FOV case. So the contribution of the Zernike surface can be expressed as

$$\begin{aligned} \vec{\delta}_{m/n} &= \frac{(n_2-n_1)}{\lambda}\sqrt{C_m^2+C_n^2}\,e^{i\arctan\left(\frac{C_n}{C_m}\right)} Z(\vec{\rho}') \\ &= \vec{V}_{m/n}\cdot Z(\vec{\rho}+\Delta\vec{h}), \end{aligned} \tag{3}$$

where n_1 and n_2 denote the refractive index of the front and the back surface, respectively. In the reflective case, the surface is in air so that $n_1 = -n_2 = 1$. $\vec{V}_{m/n}$ denotes the surface coefficient vector calculated by corresponding Zernike terms. Based on the theoretical basis above, the induced astigmatism and coma can be integrated as Eq. (4) when the Fringe Zernike terms, up to the ninth, are added to the nonstop surface:

$$\begin{aligned} {}_{\mathrm{FZ}}W_{\mathrm{asti+coma}} = {} & \vec{V}_{5/6}\cdot\vec{\rho}^2 + 3\Delta h\vec{V}_{7/8}\vec{H}\cdot\vec{\rho}^2 + 3(\vec{V}_{7/8}\cdot\vec{\rho})(\vec{\rho}\cdot\vec{\rho}) \\ & + 12\vec{V}_9\Delta h^2\vec{H}^2\cdot\vec{\rho}^2 + 24\Delta h\vec{V}_9(\vec{H}\cdot\vec{\rho})(\vec{\rho}\cdot\vec{\rho}). \end{aligned} \tag{4}$$

The first term is the field constant astigmatism induced by $C_{5/6}$. The second and third terms are the field-linear astigmatism and field constant coma, respectively, which are induced by $C_{7/8}$. The C_9 term induces the field quadratic astigmatism and field-linear coma. With the higher-order Zernike terms being used, the field-dependent behavior becomes more complex.

When the freeform surfaces are added to an off-axis optical system, the departure of the freeform surfaces from a spherical surface can be treated as a thin plate without power. The contribution to the net aberration fields is not dependent on the system's first-order parameters, but on the intersection height of the optical axis ray (OAR) with respect to the freeform vertex [9]. The concept of the off-axis freeform aberration field distribution is demonstrated in Fig. 1. According to Thompson's VAT [5], when a spherical surface tilts by an angle of ω, the

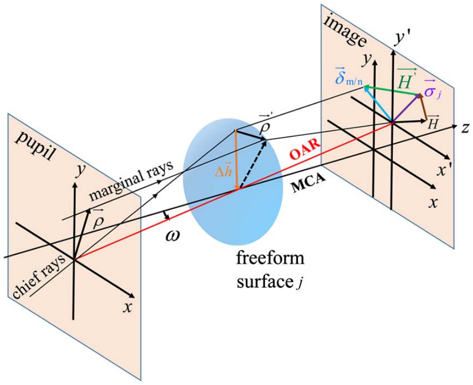

Fig. 1. Concept of off-axis freeform aberration field distribution.

OAR which determines the field center on the Gaussian image plane, is no longer coincident with the mechanic coordinate axis (MCA). The center of the aberration field would move away from the coaxial aberration field center because of the vector $\vec{\sigma}_j$. If Zernike terms are added to a nonstop surface in this off-axis system, the freeform contribution, indicated as $\vec{\delta}_{m/n}$, will be the projection of the $\vec{\rho}'$ on the image field that is already displaced by the off-axis situation. Therefore, the total aberration field distribution of an off-axis freeform system is modified by the combination of vector $\vec{\sigma}_j$ and $\vec{\delta}_{m/n}$.

Various Fringe Zernike terms will induce diverse aberration contributions, so the total wave aberration of off-axis freeform system should be analyzed according to each Zernike term. First, discussion starts from the Zernike $C_{5/6}$ terms. The third-order astigmatism of an off-axis system with $C_{5/6}$ terms can be expressed as

$$\begin{aligned} {}_{5/6}W_{\text{asti}} &= \frac{1}{2}\sum W_{222_j}[(\vec{H}-\vec{\sigma}_j)^2\cdot\vec{\rho}^2]+\vec{V}_{5/6}\cdot\vec{\rho}^2 \\ &= \frac{1}{2}W_{222}[(\vec{H}-{}_{\text{tilt}}\vec{a}_{222})^2+{}_{\text{tilt}}\vec{b}^2_{222}+{}_{5/6}\vec{b}^2_{222}]\cdot\vec{\rho}^2 \\ &= \frac{1}{2}W_{222}[(\vec{H}-{}_{\text{tilt5/6}}\vec{a}_{222})^2+{}_{\text{tilt5/6}}\vec{b}^2_{222}]\cdot\vec{\rho}^2, \end{aligned} \quad (5)$$

where

$$\begin{cases} {}_{\text{tilt5/6}}\vec{a}_{222} = {}_{\text{tilt}}\vec{a}_{222} \equiv \dfrac{\sum W_{222_j}\vec{\sigma}_j}{W_{222}}, \\ {}_{5/6}\vec{b}^2_{222} = \dfrac{2\vec{V}_{5/6}}{W_{222}}, \\ {}_{\text{tilt}}\vec{b}^2_{222} = \dfrac{\sum W_{222_j}\vec{\sigma}^2_j}{W_{222}} - {}_{\text{tilt}}\vec{a}^2_{222}. \end{cases} \quad (6)$$

As the field quadratic dependence behavior shown in Eq. (5), there will be two astigmatic nodes through the aberration field. Here, ${}_{\text{tilt5/6}}\vec{a}_{222}$ denotes a normalized vector from the center of the field to the midpoint between the two astigmatic nodes. From Eq. (6), it can be seen that ${}_{\text{tilt5/6}}\vec{a}_{222}$ is the same as the vector ${}_{\text{tilt}}\vec{a}_{222}$ that was defined in Ref. [5]. It means that the $C_{5/6}$ terms in an off-axis system do not modify the location of the midpoint between the two astigmatic nodes, but the two nodes are located at the two normal components of the vector ${}_{\text{tilt5/6}}\vec{b}_{222}$, which is calculated by including both $\vec{\sigma}_j$ and $\vec{V}_{5/6}$. The nodal properties of the off-axis freeform system analyzed above are discovered for the first time and they are essential information for controlling the aberration nodes during the off-axis freeform design.

The two-mirror coaxial system with stop located at the primary mirror is built to validate the derivations above, shown in Fig. 2. Furthermore, in order to demonstrate the distribution properties of the aberration field directly, the FFDs generated by CODE V are utilized to display the nodal aberration field behavior. Since FFDs are based on the real ray-tracing data without freeform aberration theory, it is an excellent validation of the theoretical developments [10,11].

Figure 3 shows the astigmatism field map in FFDs. For simplicity, it is assumed that only the primary mirror tilts just about the sagittal direction. Consequently, two astigmatic nodes can be found on the field y axis, shown in Fig. 3(a). This situation had been explained by Thompson [5]. If the $C_{5/6}$ terms are added to the secondary mirror in the coaxial system, binodal astigmatism will be located at both symmetrical sides of ${}_{5/6}\vec{b}_{222}$ calculated in Eq. (6), shown in Fig. 3(b). While the $C_{5/6}$ terms are added to the secondary mirror of the case (a), the nodal locations in the field map are shown in Fig. 3(c). It can be seen that the binodal astigmatism response still remains, but the locations are redistributed. The midpoint of the two nodes does not move compared to case (a). As a result, the nodal locations are still symmetric about the field y axis, but the distance between the two nodes is recomputed by the vector ${}_{\text{tilt5/6}}\vec{b}_{222}$. Figure 3 validates that the distribution of astigmatic nodes is coincident with the derivation in Eq. (5).

Next, the aberration distribution caused by the $C_{7/8}$ terms, which will not only lead to a change in astigmatism distribution, but also in coma distribution, is discussed. When the $C_{7/8}$ terms are added to the tilted nonstop surface, the third-order astigmatism is computed by

$$\begin{aligned} {}_{7/8}W_{\text{asti}} &= \frac{1}{2}\sum W_{222_j}[(\vec{H}-\vec{\sigma}_j)^2\cdot\vec{\rho}^2]+3\Delta h\vec{V}_{7/8}\vec{H}\cdot\vec{\rho}^2 \\ &= \frac{1}{2}W_{222}[(\vec{H}-{}_{\text{tilt7/8}}\vec{a}_{222})^2+{}_{\text{tilt7/8}}\vec{b}^2_{222}]\cdot\vec{\rho}^2. \end{aligned} \quad (7)$$

In this case, since the highest-order field dependence in the equation has not changed compared to the third-order astigmatism, the astigmatic field still contains two nodes properties.

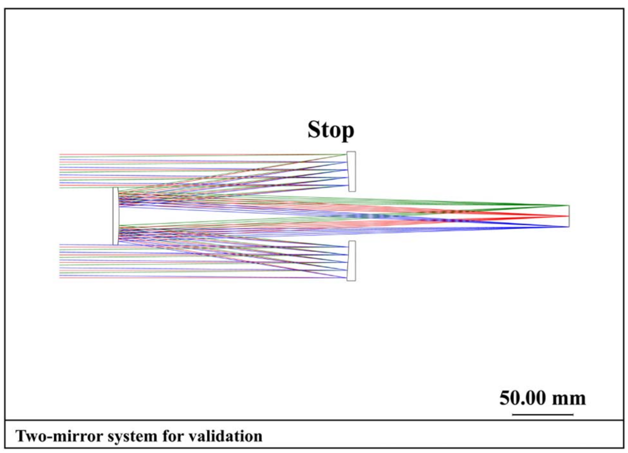

Fig. 2. Optical layout of the two-mirror system for validation.

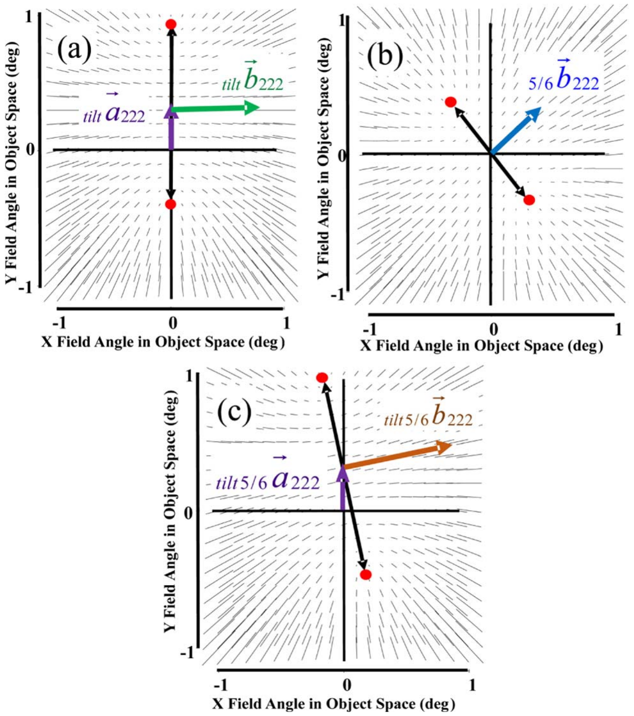

Fig. 3. Binodal astigmatism response for the case of (a) tilting the primary mirror 2° in the sagittal plane, (b) adding freeform ($C_5 = 0$, $C_6 = 1\times10^{-6}$) to the secondary mirror in the coaxial system, and (c) adding the freeform of case (b) in the off-axis system of case (a). The field angles have been normalized and the following is the same.

However, it is worth noting that the midpoint between the two nodes has moved on account of the field-linear astigmatism induced by the $C_{7/8}$ terms. The midpoint location is calculated as

$$_{\mathrm{tilt}7/8}\vec{a}_{222} = {}_{\mathrm{tilt}}\vec{a}_{222} + \frac{1}{2}{}_{7/8}\vec{b}_{222}, \tag{8}$$

where

$$_{7/8}\vec{b}_{222} = \frac{-6\Delta h\vec{V}_{7/8}}{W_{222}}. \tag{9}$$

The certain positions of the two nodes are located at both symmetric sides of vector $_{\mathrm{tilt}7/8}\vec{b}_{222}$. As shown in Eq. (10), the vector is determined by the combination of the field decentration vector and surface coefficient vector:

$$_{\mathrm{tilt}7/8}\vec{b}^2_{222} = {}_{\mathrm{tilt}}\vec{b}^2_{222} - \left({}_{\mathrm{tilt}}\vec{a}_{222} + \frac{1}{2}{}_{7/8}\vec{b}_{222}\right)^2. \tag{10}$$

Figure 4(a) shows the binodal astigmatism response induced by the $C_{7/8}$ terms in a coaxial system, which had been analyzed by Yang *et al.* [6]. When the $C_{7/8}$ terms are added to the secondary mirror in the case of Fig. 3(a), the midpoint between the two nodes moves away from the field y axis, and the two nodes are not symmetric about the field y axis anymore, as shown in Fig. 4(b).

The third-order coma of an off-axis system that has added Zernike $C_{7/8}$ terms to the nonstop surface can be expressed as

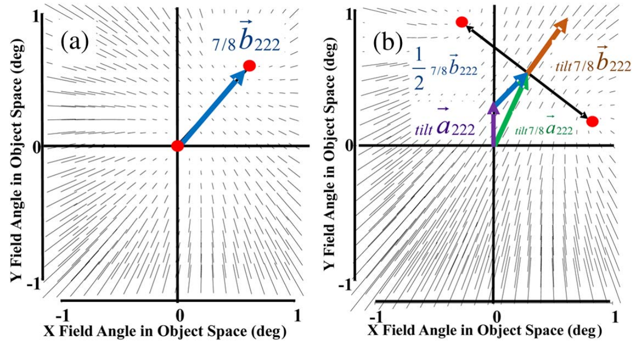

Fig. 4. Astigmatic field map of case (a) when freeform ($C_7 = -1\times10^{-7}$, $C_8 = -1\times10^{-7}$) is added to the secondary mirror in the coaxial system, (b) when the freeform ($C_{7/8}$) of case (a) is added to the secondary mirror, and the primary mirror is tilted 2°.

$$\begin{aligned} {}_{7/8}W_{\mathrm{coma}} &= \sum W_{131_j}[(\vec{H}-\vec{\sigma}_j)\cdot\vec{\rho}](\vec{\rho}\cdot\vec{\rho}) + 3(\vec{V}_{7/8}\cdot\vec{\rho})(\vec{\rho}\cdot\vec{\rho}) \\ &= [W_{131}(\vec{H} - {}_{\mathrm{tilt}}\vec{a}_{131} - {}_{7/8}\vec{a}_{131})\cdot\vec{\rho}](\vec{\rho}\cdot\vec{\rho}) \\ &= [W_{131}(\vec{H} - {}_{\mathrm{tilt}7/8}\vec{a}_{131})\cdot\vec{\rho}](\vec{\rho}\cdot\vec{\rho}), \end{aligned} \tag{11}$$

where

$$_{\mathrm{tilt}}\vec{a}_{131} \equiv \frac{\sum W_{131_j}\vec{\sigma}_j}{W_{131}}, \tag{12}$$

is a normalized vector. It determines the coma node position in an off-axis system, which was defined by Eq. (4.8) in Ref. [5]. Since the contribution of the $C_{7/8}$ terms is field-independent [6], the total coma distribution remains field-linear. It can be seen from Eq. (11) that only one coma node can be developed in this case. However, the node will shift to a new location, which is given by

$$\vec{H} = {}_{\mathrm{tilt}}\vec{a}_{131} + {}_{7/8}\vec{a}_{131}, \tag{13}$$

where

$$_{7/8}\vec{a}_{131} = \frac{3\vec{V}_{7/8}}{W_{131}}. \tag{14}$$

For the two-mirror system example, when the primary mirror tilts about the sagittal direction, the single coma node shifts along the orientation of vector $\vec{\sigma}_j$ from the original field center, shown in Fig. 5(a). If the $C_{7/8}$ terms are added to the coaxial case, the coma node is located at the endpoint of $_{7/8}\vec{a}_{131}$, shown in Fig. 5(b). Furthermore, the resultant combination of primary mirror tilt and $C_{7/8}$ terms on the secondary mirror is then shown in Fig. 5(c). It can be noted that the field dependence of the coma is essentially unchanged compared with the Figs. 5(a) and 5(b), but the coma node is displaced according to the combination of field decentration vector and the freeform surface coefficients.

Next, the aberration distributions due to inducing the Zernike C_9 term to the off-axis system are investigated. It is shown from Eq. (4) that adding a C_9 term to a nonstop surface in a coaxial system will induce field quadratic astigmatism and a field-linear coma. As the field dependence of these induced aberrations is the same as that of the corresponding third-order

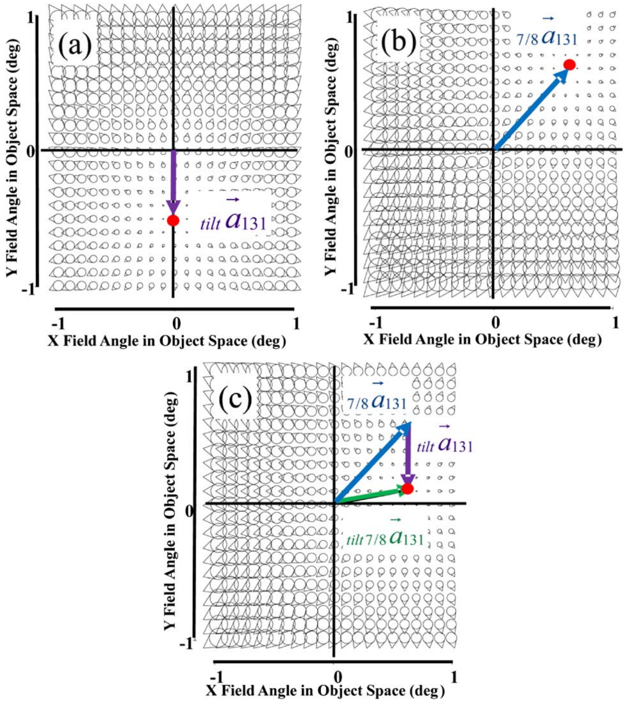

Fig. 5. Coma field map for the case of (a) tilting the primary mirror 0.2° in the sagittal plane, (b) adding freeform ($C_7 = 3 \times 10^{-8}$, $C_8 = 3 \times 10^{-8}$) to the secondary mirror in the coaxial system, and (c) adding the freeform of case (b) in the off-axis system of case (a).

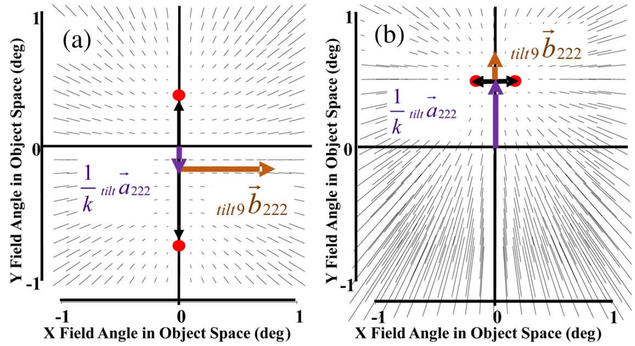

Fig. 6. Binodal astigmatism distribution when the primary mirror tilts 1° and the secondary mirror converts to the freeform with the C_9 term, (a) two nodes located on the field y axis when $|\frac{1}{k}\,_{\mathrm{tilt}}\vec{b}^2_{222}| > |(\frac{k-1}{k^2})\,_{\mathrm{tilt}}\vec{a}^2_{222}|$, otherwise located symmetrically with respect to the field y axis as (b) shown.

aberrations in a coaxial system, the node is still located at the center of each aberration field [4,6]. However, if the C_9 term is added to an off-axis system, the location properties of aberration nodes will be transformed accordingly. First, the third-order astigmatism distribution will be converted into

$$
\begin{aligned}
{}_9W_{\mathrm{asti}} &= \frac{1}{2}\sum W_{222_j}[(\vec{H}-\vec{\sigma}_j)^2\cdot\vec{\rho}^2] + 12V_9\Delta h^2\vec{H}^2\cdot\vec{\rho}^2 \\
&= \frac{1}{2}kW_{222}[(\vec{H}-\frac{1}{k}\,_{\mathrm{tilt}}\vec{a}_{222})^2 \\
&\quad + \frac{1}{k}(\,_{\mathrm{tilt}}\vec{b}^2_{222} + \left(\frac{k-1}{k}\right)\,_{\mathrm{tilt}}\vec{a}^2_{222})]\cdot\vec{\rho}^2 \\
&= \frac{1}{2}kW_{222}[(\vec{H}-\frac{1}{k}\,_{\mathrm{tilt}}\vec{a}_{222})^2 + \,_{\mathrm{tilt9}}\vec{b}^2_{222}]\cdot\vec{\rho}^2, \qquad (15)
\end{aligned}
$$

where $k = 1 + \frac{24\Delta h^2 V_9}{W_{222}}$ is a scalar that is irrelevant to the aberration field decentration vector. Referring to Eq. (15), the binodal astigmatism response can still be found, and the orientation pointing to the midpoint from the field center is solely governed by the aberration field vector $_{\mathrm{tilt}}\vec{a}_{222}$, while the magnitude is computed involving the C_9 term. Figure 6 shows the FFDs of the third-order astigmatism when the C_9 term is added to the secondary mirror and the primary mirror is tilted. Since the surface tilts only about the sagittal direction, the midpoint between the two nodes is located at the field y axis, but shifts away from the field center. If $|\frac{1}{k}\,_{\mathrm{tilt}}\vec{b}^2_{222}| > |(\frac{k-1}{k^2})\,_{\mathrm{tilt}}\vec{a}^2_{222}|$, the two nodes will be located on the field y axis, shown in Fig. 6(a). Otherwise, the nodes will be located at two symmetric sides of the field y axis, shown in Fig. 6(b).

Finally, the total third-order coma distribution of an off-axis system with a C_9 term freeform surface is computed as

$$
\begin{aligned}
{}_9W_{\mathrm{coma}} &= \sum W_{131_j}[(\vec{H}-\vec{\sigma}_j)\cdot\vec{\rho}](\vec{\rho}\cdot\vec{\rho}) \\
&\quad + 24\Delta h V_9(\vec{H}\cdot\vec{\rho})(\vec{\rho}\cdot\vec{\rho}) \\
&= W_{131}\left\{\left[\left(1+\frac{24\Delta h V_9}{W_{131}}\right)\vec{H} - \,_{\mathrm{tilt}}\vec{a}_{131}\right]\cdot\vec{\rho}\right\}(\vec{\rho}\cdot\vec{\rho}). \qquad (16)
\end{aligned}
$$

Since the field-linear behavior of the coma has not been modified, the single node property still remains. The field point goes to zero at

$$\vec{H} = \frac{1}{m}\,_{\mathrm{tilt}}\vec{a}_{131}, \qquad (17)$$

where

$$m = 1 + \frac{24\Delta h V_9}{W_{131}}. \qquad (18)$$

m is also a scalar which is calculated by the C_9 coefficient. When $m > 0$, the node is located at the orientation of the field decentration vector, otherwise, the node is located at the opposite orientation. For the two-mirror example, when the primary mirror is tilted and the C_9 term is added to the secondary mirror, the nodal point in the field map of the coma is shown in Fig. 7. Since the mirror tilts only about the sagittal direction, the coma node just produces displacement along the field y axis.

Following this method, the net aberration contribution by the rest terms of Fringe Zernike polynomials can be demonstrated. Since higher-order terms will provide higher-order field dependence, the integrated field dependence will be more complex for those higher-order aberrations. The number of nodes in the third-order aberration field will be increased accordingly. This reveals the reason that the freeform surfaces are useful in balancing high-order aberrations.

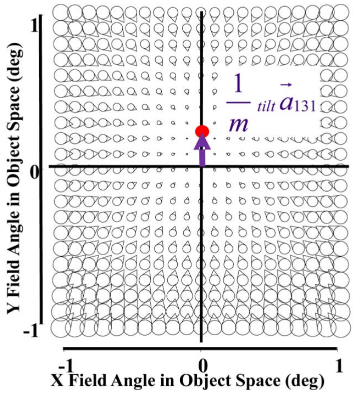

Fig. 7. Coma field map when the primary mirror is tilted 0.2° and the secondary mirror is converted into freeform ($C_9 = 1 \times 10^{-8}$).

3. DESIGN EXAMPLE

To demonstrate the applicability of the results of this work, an unobscured freeform optical system with effective focal length (EFL) of 500 mm and external pupil diameter of 300 mm is designed. The system is compatible with an uncooled focal plane array, which has a format of 384 × 288 pixels and a pixel pitch of 25 μm. So the system can provide an FOV of 1.2° × 1°. First, a suitable first-order starting point with two tilted spherical mirrors is developed based on the imaging focal length and the geometry requirements. Once the initial configuration is set up, the field distributions of the limiting aberrations are analyzed by using FFDs. Then, according to the benefits of Zernike terms discussed previously, the spherical mirrors have been converted into freeform to promote the imaging quality. During the whole process of optimizing, the system aberration nodal properties are mainly concerned, especially the third-order astigmatism and coma aberrations. The main purpose of optimization is to move the aberration nodes back into the FOV of interest by using freeform surfaces. The procedure of selecting special Zernike terms will be illustrated in detail within this section. In the last part of this section, the design results are reported.

A. First-order Geometry Computation

It begins with developing a proper initial geometry for a two-mirror system that is unobscured. Bauer designed a two-mirror freeform off-axis system with a short EFL for the electronic viewfinder [11]. Being inspired by that work, the blockage-free configuration is adopted for our design example. However, to minimize the package size of a system that contains a long EFL and a large aperture size, the image plane is restricted to be perpendicular to the entrance pupil plane, shown in Fig. 8. An off-axis initial configuration can be derived from a coaxial system. Generally, four pivotal parameters are needed to determine a coaxial two-mirror system, which are the primary mirror (PM) obscuration ratio α caused by the secondary mirror (SM), the SM magnification β, the distance between the PM vertex and the SM vertex denoted by l_1, and the distance between the SM vertex and the focus denoted by l_2. Here, l_1 and l_2 are both intended to be positive. The SM magnification can be defined by

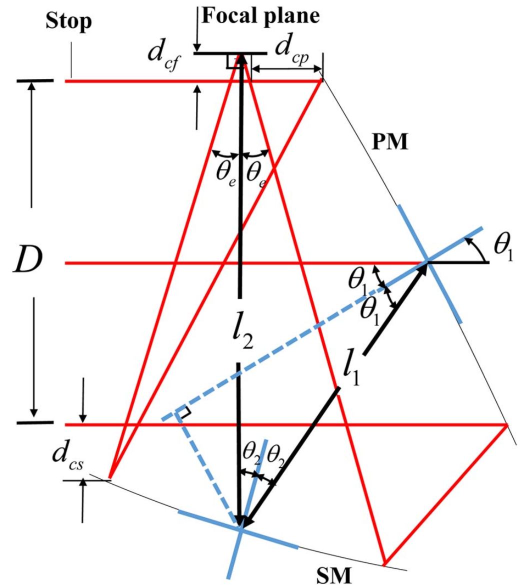

Fig. 8. Geometry of two-mirror unobscured system with design parameters.

$$\beta = \frac{f'}{f'_1}, \tag{19}$$

where f' is the effective focal length of system, and f'_1 is the focal length of the PM. By computing with the Gaussian geometry, the obscured ratio is expressed by

$$\alpha = \frac{-f'_1 + l_2 - l_1}{(\beta - 1)f'_1}, \tag{20}$$

where the distance l_1 is given by

$$l_1 = \frac{f'}{\beta}(\alpha - 1). \tag{21}$$

Therefore, the radii of PM and SM can be obtained from

$$\begin{cases} R_1 = 2f'_1, \\ R_2 = \frac{\alpha\beta}{\beta+1} R_1. \end{cases} \tag{22}$$

To obtain the blockage-free configuration, PM and SM need to be tilted by θ_1 and θ_2 with respect of their vertices at the sagittal direction, respectively. By controlling the clearances of the feature rays to the mirrors, especially d_{cs}, the distance between the lowest entrance rays and the edge of SM; d_{cf}, the distance between the top ray and the focal plane; and d_{cp}, the distance of the marginal rays that are incident to the focal plane and the edge of PM, the system structure is almost restricted, as shown in Fig. 8. On the basis of the geometrical relationship, these three important parameters are calculated by

$$\begin{cases} d_{cf} = l_2 - \left(l_1 - \frac{D}{2\sin 2\theta_1}\right)\cos 2\theta_2 - D, \\ d_{cs} = \left(l_1 - \frac{D}{2\sin 2\theta_1}\right)\cos 2\theta_2 - l_2(\sin\theta_e)^2, \\ d_{cp} = l_1 \sin 2\theta_2 - \frac{D}{2}\tan\theta_1 - d_{cf}\tan\theta_e, \end{cases} \tag{23}$$

where D is the entrance pupil diameter. θ_e represents the incident angle of the marginal rays onto the focal plane, which is related to the system relative aperture,

$$\sin 2\theta_e = D/f'. \tag{24}$$

In order to obtain a compact structure, the focal plane is located above the PM and kept perpendicular to the entrance pupil plane, which requires

$$\theta_1 + \theta_2 = \frac{\pi}{4}. \tag{25}$$

So in this case, Eq. (23) can be simplified as

$$\begin{cases} d_{cf} = l_2 - l_1 \cos 2\theta_2 - \frac{D}{2}, \\ d_{cs} = l_1 \cos 2\theta_2 - \frac{D}{2} - l_2(\sin\theta_e)^2, \\ d_{cp} = l_1 \sin 2\theta_2 - \frac{D(1-\tan\theta_2)}{2(1+\tan\theta_2)} - d_{cf}\tan\theta_e. \end{cases} \tag{26}$$

Based on these considerations above, if these three clearances have been estimated from the desired system with a certain focal length and pupil diameter, the relative tilt angles and the power distribution of these two mirrors can be adjusted. Consequently, a good initial configuration with tilted spherical mirrors is set up for optimization.

B. Design Process

Based on the discussions above, the starting parameters of the unobscured two-mirror system are listed in Table 1. Then, the first-order parameters listed in Table 2 can be yielded based on the computation in Section 3.A.

In consideration of the stray light performance and the feasibility of the structure, an external stop ahead of the PM with a distance of 300 mm is placed. Since a large pupil is required for sufficient entrance energy, the mirrors need to be tilted with large angles to form an unobscured system, shown in Table 2. Consequently, the astigmatism and coma contributions across the full FOV are nearly field-constant with about 1000 waves, shown in Fig. 9, which have become the dominant aberrations for the imaging performance [12,13]. There are limited freedom degrees of a spherical-based system with only two mirrors for balancing these residual aberrations. So the freeform surfaces are adopted to increase the degrees of freedom for optimzing the optical system. In this design example, a Fringe Zernike polynomial is utilized to characterize the shape of the freeform surfaces, which is applied in the CODE V software.

It is obvious that the aberration nodes have been moved out of the intended FOV because of the tilted mirrors. By taking the benefits of freeform surfaces discussed in Section 2, the strategy for reducing the system aberration level is to move the aberration nodes back into the field region of interest.

Table 1. Design Example Starting Parameters[a]

Parameter	f'	D	d_{cp}	d_{cf}	d_{cs}
Value	500	300	70	30	30

[a]Starting parameters are in mm.

Table 2. Design Example Computed Parameters[a]

Parameter	R_1	R_2	l_1	l_2	θ_1	θ_2
Value	−2700	1270	270	400	27.3	17.7

[a]R_1, R_2, l_1, and l_2 are in mm while θ_1 and θ_2 are in degrees.

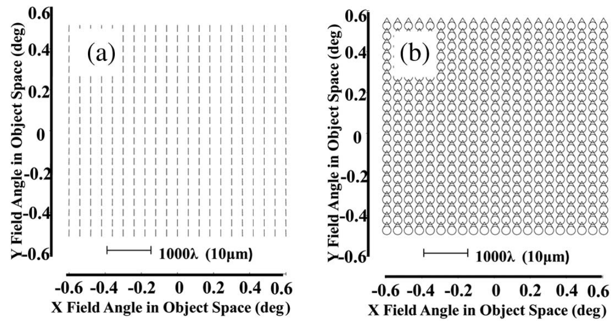

Fig. 9. Astigmatism (a) and coma (b) contributions across the full FOV after tilting the surfaces to form a representative unobscured system. Tilting the surfaces has resulted in significant amounts of a nearly field-constant coma and astigmatism with about 1000 waves.

Moreover, in order to obtain a symmetric imaging performance, the freeform coefficients should be chosen carefully. Some coefficients which will cause the asymmetrical field distribution should be avoided. For example, the C_6 and C_7 terms which are coupled with C_5 and C_8 terms should not be added to the surfaces. The aberration distribution should be focused through the FFDs during the whole process of controlling the node positions. A convenient design procedure for adding Fringe Zernike polynomial terms is introduced as follows.

From the computed parameters in Table 2, the light is mainly converged by the SM, which will cause dominant aberrations of the system. Therefore, the SM is first picked to be converted into a freeform surface. First, the C_5 term is induced to adjust the third-order astigmatism field distribution. After one round of optimization with using the damped least-squares method provided by the software, the nodes in the astigmatic field are still away from the FOV. So the C_8 term is induced to further adjust astigmatism. After another round, it can be found that the astigmatic nodes will move toward to the FOV, but they are still out of the FOV region. However, at this time, the coma node is already located at the center of the FOV. So it can be predicted that the system coma is mainly corrected by the SM. For the next round, the PM is converted into freeform by inducing the C_5 and C_8 terms. As a result, the nodes in the astigmatic and coma field both move back into the FOV region. The system astigmatism could be balanced by the PM. Now, the residual spherical aberrations become the main limiting factor. So the C_9, C_{16}, and C_{25} terms are induced to the PM and SM to reduce the aberration level. Meanwhile, the astigmatism and coma node positions are further adjusted. After inducing these terms to the mirrors, the optimized astigmatic field will have two nodes which are both on the field y axis, and the single coma node will move along the y axis accordingly. It is important to note that this kind of aberration redistribution preserves the symmetry of the imaging performance. Since the system requires a relatively large aperture, high-order aberrations cannot be ignored. The rest of the higher-order terms, such as C_{11}, C_{12}, C_{15}, C_{20}, C_{21}, C_{24}, and C_{27} are induced to the mirrors for balancing the high-order aberrations. As a consequence, the number of aberration nodes in the field will be increased. Finally, a good imaging performance can be achieved by iterative optimizations.

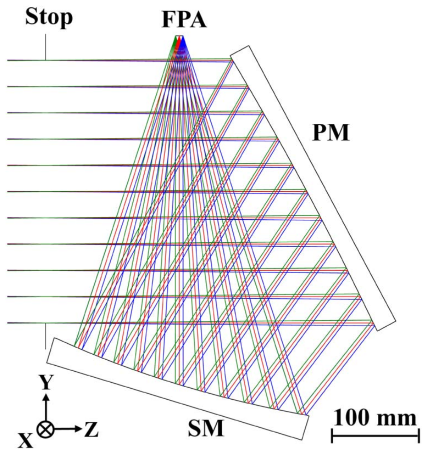

Fig. 10. Optical layout of the optimized two-mirror freeform system.

C. Design Results

The layout of the optimized two-mirror freeform system is shown in Fig. 10. The tilt angels of the two mirrors, θ_1 and θ_2, which have been optimized, are 28° and 17°, respectively. The sag difference of the freeform mirrors with respect to the basic sphere for the two mirrors is shown in Fig. 11. Through observation, it can be found that the main contribution from

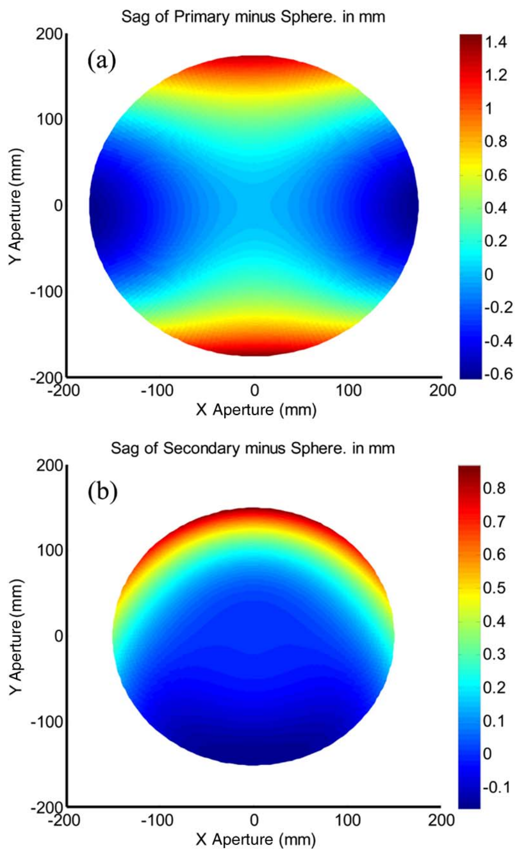

Fig. 11. Primary (a) and secondary (b) mirror sag difference with respect to the basis spherical. The maximum apertures of the primary and secondary mirrors are 350 mm and 300 mm, respectively.

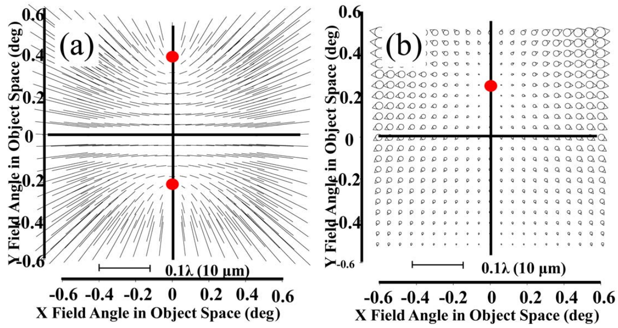

Fig. 12. Astigmatism (a) and coma (b) distribution of optimized system. The astigmatic nodes are located on the field y axis, and one of the coma nodes is back into the FOV.

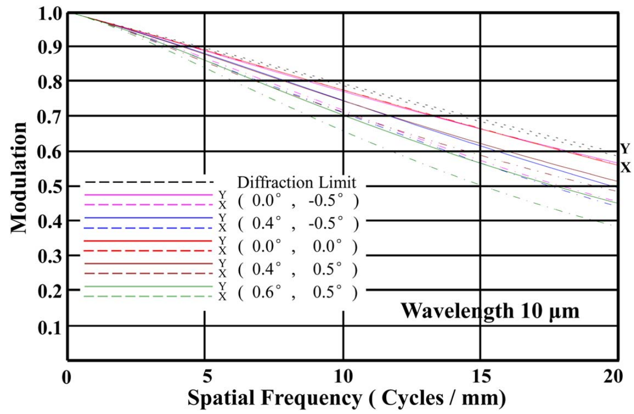

Fig. 13. MTF curves of the optimized system.

the PM is astigmatism, and the contribution from the SM is nearly a coma. Additionally, the surface shapes of the two circular apertures have been constrained to be symmetrical about the y axis to achieve a bilateral symmetrical imaging performance. The final third-order astigmatism and coma distributions are displayed in Fig. 12. It can be noted that the two nodes of astigmatism are located just on the y field axis, and one of the coma nodes is back to the FOV compared to the initial spherical case. These third-order aberrations have reduced to a low level, about 0.1 waves at 10 μm. The results of nodal locations are identical with our previous expectations. As the low-order Zernike coefficients are dominant in the optimized system, the field dependence of the third-order aberrations has not changed. When the 25 μm pitch sensor is adopted in this optical system, the resulting Nyquist frequency is 20 lp/mm, and at this frequency the MTF curves are nearly greater than 0.4, shown in Fig. 13. The final optical performance meets the imaging requirements.

4. CONCLUSION

In this paper, the distributions of the third-order aberrations were analyzed theoretically based on the NAT, especially the astigmatism and coma, with adding Fringe Zernike polynomial surfaces to an off-axis system. The nodal aberration properties of Zernike terms in a system with tilted surfaces were revealed and validated, which could provide necessary insight and guidance for off-axis aberration correction and optimization during freeform system design. It had also been revealed that introducing low-order Zernike terms to the off-axis system, such as $C_{5/6}$, $C_{7/8}$ and C_9, would not change the field dependence, but would modify the nodal positions with the combination impacts of off-axis and surface shape. Based on these analysis results, an off-axis two-mirror freeform system with an EFL of 500 mm was designed. The field-constant aberrations introduced by tilting surfaces had been balanced by specific Zernike terms. The imaging performance was bilaterally symmetric and met the requirements. This work could be of some help for optical designers to analyze the contribution of aberrations induced by the freeform surfaces.

Funding. National Natural Science Foundation of China (NSFC) (91338116, 61505201).

Acknowledgment. We thank Synopsys for providing an education license for CODE V.

REFERENCES

1. M. Rodgers, “Unobscured mirror designs,” Proc. SPIE **4832**, 33–60 (2002).
2. K. Fuerschbach, J. P. Rolland, and K. P. Thompson, “A new family of optical systems employing φ-polynomial surfaces,” Opt. Express **19**, 21919–21928 (2011).
3. F. Fang, X. Zhang, A. Weckenmann, G. Zhang, and C. Evans, “Manufacturing and measurement of freeform optics,” CIRP Ann. **62**, 823–846 (2013).
4. K. Fuerschbach, J. P. Rolland, and K. P. Thompson, “Theory of aberration fields for general optical systems with freeform surfaces,” Opt. Express **22**, 26585–26606 (2014).
5. K. P. Thompson, “Description of the third-order optical aberrations of near-circular pupil optical systems without symmetry,” J. Opt. Soc. Am. A **22**, 1389–1401 (2005).
6. T. Yang, J. Zhu, and G. Jin, “Nodal aberration properties of coaxial imaging systems using Zernike polynomial surfaces,” J. Opt. Soc. Am. A **32**, 822–836 (2015).
7. R. V. Shack and K. Thompson, “Influence of alignment errors of a telescope system on its aberration field,” Proc. SPIE **0251**, 146–153 (1980).
8. Synopsys Inc, “Zernike polynomials,” in CODE V Reference Manual (2011), Volume IV, Appendix C.
9. T. Schmid, J. P. Rolland, A. Rakich, and K. P. Thompson, “Separation of the effects of astigmatic figure error from misalignments using Nodal Aberration Theory (NAT),” Opt. Express **18**, 17433–17447 (2010).
10. R. W. Gray, C. Dunn, K. P. Thompson, and J. P. Rolland, “An analytic expression for the field dependence of Zernike polynomials in rotationally symmetric optical systems,” Opt. Express **20**, 16436–16449 (2012).
11. A. Bauer and J. P. Rolland, “Design of a freeform electronic viewfinder coupled to aberration fields of freeform optics,” Opt. Express **23**, 28141–28153 (2015).
12. K. P. Thompson, “Beyond optical design: interaction between the lens designer and the real world,” Proc. SPIE **554**, 426–438 (1985).
13. K. P. Thompson, “Aberration fields in tilted and decentered optical systems,” Ph.D. dissertation (University of Arizona, 1980).